Available online at www.sciencedirect.com
SCIENCE DIRECT
International Journal of Pressure Vessels and Piping 83 (2006) 161–167
INTERNATIONAL JOURNAL OF Pressure Vessels and Piping
www.elsevier.com/locate/ijpvp

Ultimate analysis of PWR prestressed concrete containment subjected to internal pressure

Hsuan-Teh Hu *, Yu-Hon Lin

Department of Civil Engineering, National Cheng Kung University, 1 University Road, Tainan 701, Taiwan, ROC

Received 27 July 2004; received in revised form 24 January 2006; accepted 6 February 2006

Abstract

Numerical analyses are carried out by using the ABAQUS finite element program to predict the ultimate pressure capacity and the failure mode of the PWR prestressed concrete containment at Maanshan nuclear power plant. Material nonlinearity such as concrete cracking, tension stiffening, shear retention, concrete plasticity, yielding of prestressing tendon, yielding of steel reinforcing bar and degradation of material properties due to high temperature are all simulated with proper constitutive models. Geometric nonlinearity due to finite deformation has also been considered. The results of the analysis show that when the prestressed concrete containment fails, extensive cracks take place at the apex of the dome, the junction of the dome and cylinder, and the bottom of the cylinder connecting to the base slab. In addition, the ultimate pressure capacity of the containment is higher than the design pressure by 86%.

Keywords: Ultimate analysis; Pressurized water reactor; Prestressed concrete containment; Internal pressure

1. Introduction

Since the accident at Three Mile Island nuclear plant in 1979, it has become necessary to perform failure analysis and calculate the ultimate pressure capability of the nuclear reactor containment for the safety assessment of nuclear power plants [1–3]. The containment structures in service at Taiwan, ROC were built in the late 1970 or early 1980. Since then, nonlinear material constitutive models and nonlinear finite element solution techniques have been continuously and successfully developed [4–12]. Therefore, it is possible to predict the ultimate pressure capability of the nuclear reactor containment more accurately than before by utilizing the nonlinear finite element method [13–15]. The Atomic Energy Council (AEC) at Taiwan, ROC has run several studies toward the failure analysis of containment structures. As one of the research projects sponsored by AEC, the aim of this paper is to employ the nonlinear finite element program ABAQUS [16] to investigate the ultimate pressure capacity and the failure mode of the pressurized water reactor (PWR) prestressed concrete containment at Maanshan nuclear power plant, Taiwan, ROC.

In the paper, the geometry and finite element mesh of the containment are reviewed first. Then, material properties of reinforcing steel bar, prestressing tendon and concrete are given and proper constitutive models are introduced to simulate the nonlinear behaviour of these materials such as concrete cracking, tension stiffening, shear retention, concrete plasticity, yielding of reinforcing steel bar, yielding of prestressing tendon and degradation of material properties due to high temperature. Finally, failure analyses of the containment subjected to internal pressure are carried out and important conclusions are given.

2. Containment geometry and finite element mesh

The PWR prestressed concrete containment at Maanshan nuclear power plant is composed of a circular base slab, an upright cylinder and a hemispherical dome (Fig. 1). To simplify the analysis, the tendon gallery, equipment hatches and penetrations on the containment are not considered and the structural geometry is assumed to be axisymmetric. The base slab of the containment is embedded in the soil and the dimensions of the containment are shown in Fig. 1.

At the cylinder wall, the prestressing tendons are placed in the meridional and circumferential directions of the containment. At the dome, the prestressing tendons are placed

* Corresponding author. Tel.: +886 6 2757575x63168; fax: +886 6 2358542.
E-mail address: hthu@mail.ncku.edu.tw (H.-T. Hu).

0308-0161/$ - see front matter © 2006 Elsevier Ltd. All rights reserved.
doi:10.1016/j.ijpvp.2006.02.030

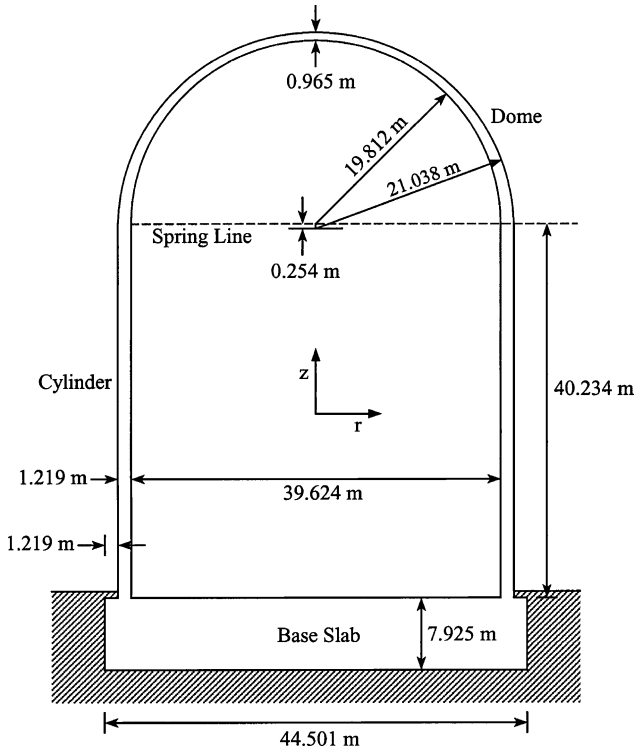

Fig. 1. Geometry and dimensions of the PWR prestressed concrete containment of Maanshan nuclear power plant.

in the circumferential direction and the directions parallel to x- and y-coordinates (Fig. 2(a)). Most of the steel reinforcing bars are placed in an axisymmetric manner in the containment but some steel reinforcement layers near the apex of the dome and in the base slab are placed in the directions parallel to the x- and y-axes. Because some prestressing tendons and some steel reinforcing bars are not placed axisymmetrically, the deformation of the containment is no longer axisymmetric and has four planes of symmetry (Fig. 2(a)). As a result, only 1/8 part of the structure is analyzed and the boundary conditions imposed on the symmetry planes are displacements in the circumferential direction, rotations in the radial direction and rotations in the z-direction to be zero. For simplicity, the lateral pressure applied to the base slab due to soil is not considered.

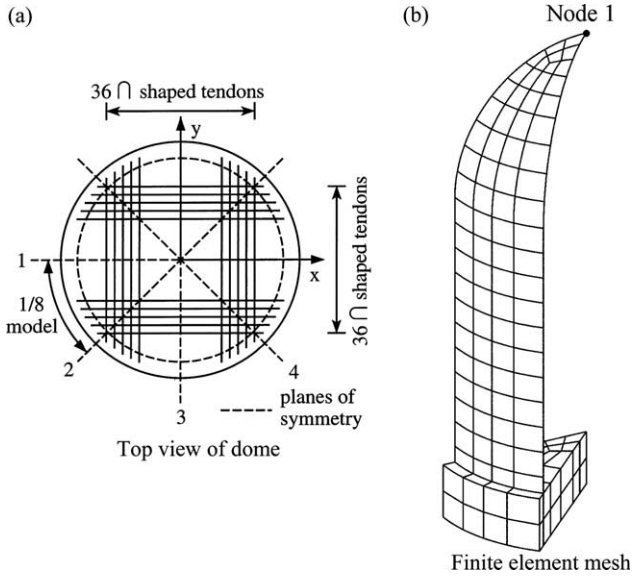

Fig. 2. 1/8 model of the PWR prestressed concrete containment of Maanshan nuclear power plant.

In the numerical simulation, eight-node shell elements (six degrees of freedom per node) are used to model the parts of the dome and cylinder. The formulation of the eight-node shell allows transverse shear deformation and these shear flexible shell elements can be used for both thick and thin shell analysis [16]. While 20-node solid elements (three degrees of freedom per node) are used to model the base slab (Fig. 2(b)), special purpose gap elements are used to link the bottom of the base slab to the ground. The gap elements allow the contact surfaces between the base slab and the ground to remain closed or open but not to penetrate each other.

3. Material properties and constitutive models

The structural materials used in the containment can be divided into three groups, which are steel reinforcing bar, prestressing tendon and concrete. The bond between steel and concrete is assumed to be perfect. The material properties of all the materials and their constitutive models used by ABAQUS are briefly discussed in the following sections.

3.1. Steel reinforcing bar

The reinforcement used in the containment structure is ASTM A-615 Grade 60 steel with yield stress

$$\sigma_y = 413.7 \text{ MPa} \tag{1}$$

and its elastic modulus is assumed to be [17]

$$E_s = 200 \text{ GPa} \tag{2}$$

The stress–strain curve of the reinforcing bar is assumed to be elastic-perfectly plastic.

3.2. Prestressing tendon

The prestressing tendon used in the containment is composed of 37 Grade 250 strands. The diameter of each strand is 1.52 cm. The average tensile force is 6552 kN for the tendons in the meridian direction and is 6775 kN for the tendons in the circumferential direction. Due to the lack of material test data, the nonlinear stress–stain curve of the strand given by Nilson and Winter [18] is adopted and simplified to a piecewise linear curve as shown in Fig. 3. In addition, the elastic modulus of the tendon is assumed to be:

$$E_s = 189.6 \text{ GPa} \tag{3}$$

In ABAQUS, the prestressing tendon and the steel reinforcement are treated as equivalent uniaxial materials, which are smeared through the element section. In order to properly model the constitutive behaviours of the tendon and the reinforcement, the cross sectional area, spacing, position

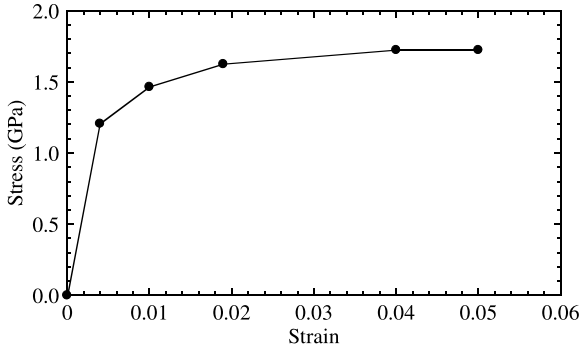

Fig. 3. Stress–strain curve for prestressing tendon.

and orientation of each layer of tendon or steel bar within each element need to be specified.

3.3. Concrete

The concrete used in the containment structure has an uniaxial compressive strength f_c' given as

$$f_c' = 34.47 \text{ MPa} \tag{4}$$

Under uniaxial compression, the concrete strain ε_0 corresponding to the peak stress f_c' is usually around the range of 0.002–0.003. A representative value suggested by ACI Committee 318 [17] is:

$$\varepsilon_0 = 0.003 \tag{5}$$

The Poisson's ratio ν_c of concrete under uniaxial compressive stress ranges from about 0.15 to 0.22, with a representative value of 0.19 or 0.20 [8]. In this study, the Poisson's ratio of concrete is assumed to be

$$\nu_c = 0.2 \tag{6}$$

The uniaxial tensile strength f_c' of concrete is difficult to measure and is normally taken as [8]:

$$f_t' = 0.33\sqrt{f_c'} \quad \text{MPa} \tag{7}$$

The initial modulus of elasticity of concrete E_c is highly correlated to its compressive strength and can be calculated with reasonable accuracy from the empirical equation [17]:

$$E_c = 4700\sqrt{f_c'} \quad \text{MPa} \tag{8}$$

It should be noted that in Eqs. (7) and (8) the unit of f_c' is in MPa.

Under different combinations of loading, the failure strengths of concrete are different from that under uniaxial condition. However, the maximum strength envelope under multiple stress conditions seems to be largely independent of load path [19]. In ABAQUS, a Mohr–Coulomb type compression surface combined with a crack detection surface are used to model the failure surface of concrete (Fig. 4). When the principal stress components of concrete are dominantly compressive, the response of concrete is modeled by an elastic–plastic theory with associate flow and isotropic hardening rule. In tension, once cracking is defined to occur

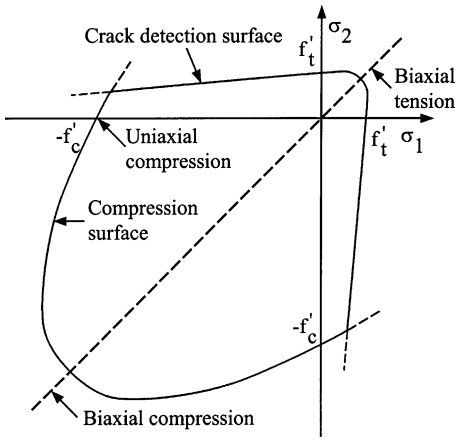

Fig. 4. Concrete failure surface in plane stress.

(by the crack detection surface), the orientation of the cracks is stored. Damaged elasticity is then used to model the existing cracks.

When plastic deformation occurs, there should be a certain parameter to guide the expansion of the yield surface. A commonly used approach is to relate the multidimensional stress and strain conditions to a pair of quantities, namely, the effective stress σ_c and effective strain ε_c, such that results obtained following different loading paths can all be correlated by means of the equivalent uniaxial stress–strain curve. The stress–strain relationship proposed by Saenz [20] has been widely adopted as the uniaxial stress–strain curve for concrete and it has the following form

$$\sigma_c = \frac{E_c\varepsilon_c}{1 + (R + R_E - 2)\left(\frac{\varepsilon_c}{\varepsilon_0}\right) - (2R-1)\left(\frac{\varepsilon_c}{\varepsilon_0}\right)^2 + R\left(\frac{\varepsilon_c}{\varepsilon_0}\right)^3} \tag{9}$$

where

$$R = \frac{R_E(R_\sigma - 1)}{(R_\varepsilon - 1)^2} - \frac{1}{R_\varepsilon}, \quad R_E = \frac{E_c}{E_0}, \quad E_0 = \frac{f_c'}{\varepsilon_0}$$

and $R_\sigma = 4$, $R_\varepsilon = 4$ may be used [11]. In the analysis, Eq. (9) is taken as the equivalent uniaxial stress–strain curve for concrete and approximated by several piecewise linear segments as shown in Fig. 5.

When cracking of concrete takes place, a smeared model is used to represent the discontinuous macrocrack behaviour. It is

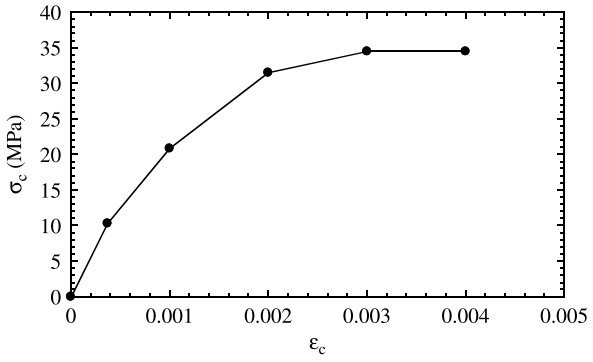

Fig. 5. Equivalent uniaxial stress–strain curves for concrete.

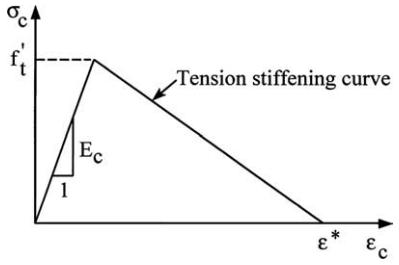

Fig. 6. Tension stiffening model.

known that the cracked concrete of a reinforced concrete element can still carry some tensile stress in the direction normal to the crack, which is termed tension stiffening [8]. In this study, a simple descending line is used to model this tension stiffening phenomenon (Fig. 6). The default value of the strain ε^* at which the tension stiffening stress reduced to zero is [16]:

$$\varepsilon^* = 0.001 \tag{10}$$

During the postcracking stage, the cracked reinforced concrete can still transfer shear forces through aggregate interlock or shear friction, which is termed shear retention [8]. Assume the shear modulus of intact concrete is G_c. The reduced shear modulus $\hat{G}$ of cracked concrete can be expressed as

$$\hat{G} = \mu G_c \tag{11a}$$

and

$$\mu = 1 - \varepsilon/\varepsilon_{max} \tag{11b}$$

where ε is the strain normal to the crack direction and ε_{max} is the strain at which the parameter μ reduces to zero (Fig. 7). In ABAQUS, ε_{max} is usually assumed to be a very large value, i.e. $\mu = 1$ (full shear retention). In this investigation, other than specified, the default values for tension stiffening parameter $\varepsilon^* = 0.001$ and for shear retention parameter $\varepsilon^* = 1$ are used.

3.4. Material properties at elevated temperature

All the aforementioned material properties for steel and concrete are tested or assumed under room temperature conditions. In the case of a nuclear accident, the containment will usually be subjected to elevated temperature and internal pressure. Therefore, the degradation of material properties due to high temperature should be considered. Owing to the material properties of Maanshan nuclear power plant at elevated temperatures being unavailable, the ratios of material

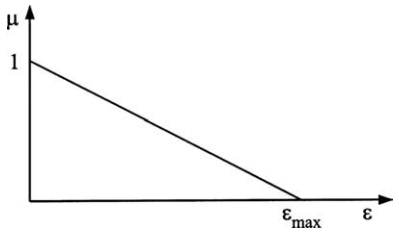

Fig. 7. Shear retention parameter.

Table 1
Material properties for concrete and steel at various temperatures [22]

Materials	Temperatures (°C)		
	21	121	371
Concrete			
Young's modulus E_c (GPa)	33.1	15.9	8.3
Poisson's ratio ν_c	0.2	0.2	0.2
Tensile strength f_t' (MPa)	3.44	2.43	1.72
Compressive strength f_c' (MPa)	46.9	33.1	23.4
Strain at compressive strength ε_0	0.0023	0.00297	0.00372
Steel			
Young's modulus E_s (GPa)	214	197	177
Yield stress σ_y (MPa)	459	390	354
Ultimate stress σ_u (MPa)	683	628	492
Strain at ultimate stress	0.045	0.045	0.045

properties at elevated temperature to those at room temperature as given in Table 1 [21] are used to linearly scale down the material properties in the high temperature analyses. The material properties used in analysis in the room temperature (21 °C) condition and at elevated temperature (121 and 371 °C) conditions are given in Table 2. In this paper, other than specified, all the analyses are assumed to be carried out at the room temperature (21 °C) condition.

4. Numerical analysis

4.1. Ultimate analysis of the PWR containment subjected to internal pressure

The loads applied to the containment include the prestressing forces from the tendons and the internal pressure. In the finite element analysis, the prestressing forces from the tendons are simulated with initial stresses and applied to the containment first. After the structure is in an equilibrium condition, the internal pressure p is then applied to the containment up to failure. According to the Final Safety Analysis Report [22], the

Table 2
Material properties used for PWR prestressed concrete containment in numerical analysis

Materials	Temperatures (°C)		
	21	121	371
Concrete			
Young's modulus E_c (GPa)	27.79	13.31	6.95
Poisson's ratio ν_c	0.2	0.2	0.2
Tensile strength f_t' (MPa)	1.95	1.38	0.97
Compressive strength f_c' (MPa)	34.47	24.33	17.24
Strain at compressive strength ε_0	0.003	0.00387	0.00485
Tension stiffening parameter ε^*	0.001	0.001	0.001
Shear retention parameter μ	1	1	1
Reinforcing bar			
Young's modulus E_s (GPa)	199.9	183.8	165.8
Yield stress σ_y (MPa)	413.7	351.6	318.5
Prestressing tendon			
Young's modulus E_s (GPa)	189.6	174.3	157.1
Yield stress σ_y (MPa)	1207	1025	929
Ultimate stress σ_u (MPa)	1724	1486	1241
Strain at ultimate stress σ_u	0.05	0.05	0.05

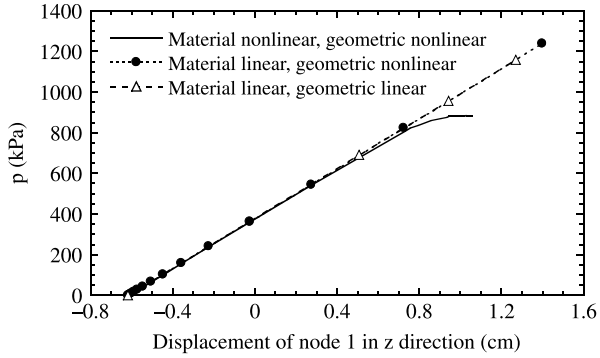

Fig. 8. Influence of material nonlinearity and geometric nonlinearity on the ultimate pressure capacity of containment.

containment accident pressure load is 414 kPa, which is greater than the calculated peak pressure 338 kPa occurring as the result of any rupture of the reactor coolant system or main steam system. To fulfill the requirements of NRC Regulatory 1.18, the accident pressure load is further multiplied by a factor 1.15 to obtain a design pressure load 476 kPa [22].

Fig. 8 shows the internal pressure p versus the displacement of node 1 (at the apex of the containment) in the z-direction by considering different combinations of material nonlinearity and geometric nonlinearity. When both material nonlinearity and geometric nonlinearity are considered, the ultimate internal pressure p_u of the containment is 886 kPa, which is about 86% higher than the design pressure 476 kPa. The deformation shape of the containment under the ultimate internal pressure condition is shown in Fig. 9(a) and the crack patterns of the concrete at the inner and outer sides of the containment are shown in Fig. 9(b). From these figures we can observe that

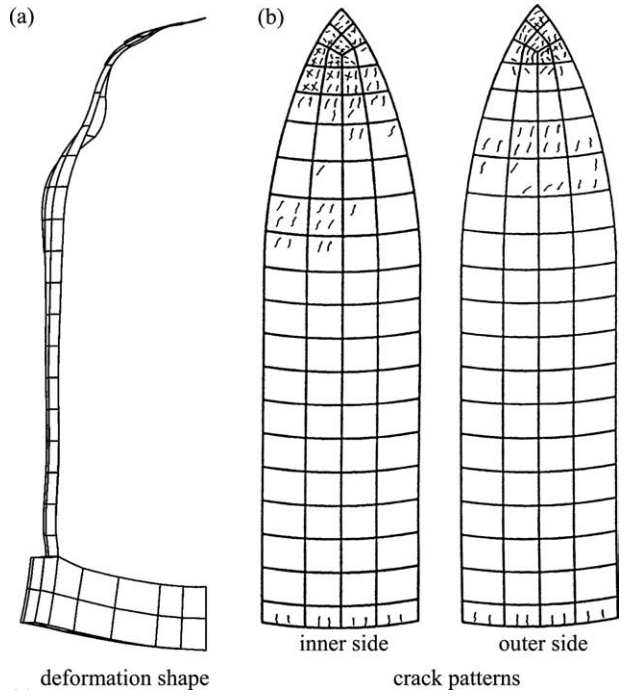

Fig. 9. Deformation shape and crack patterns of containment at the ultimate internal pressure $p_u = 886$ kPa.

under the ultimate pressure, the base slab tends to lift. Most of the deformations take place in the dome. In addition, because of the stress concentration, cracks are likely to occur near the apex of the dome, the junction of the dome and cylinder, and the bottom of the cylinder.

4.2. Influence of material nonlinearity and geometric nonlinearity on the ultimate pressure capacity of containment

Fig. 8 shows the load–displacement curves of node 1 by considering different combinations of material nonlinearity and geometric nonlinearity. When all the materials of the containment, i.e. concrete, steel reinforcing bar and prestressing tendon, have a linear elastic response, the result of analysis (with $p < 1400$ kPa) by employing the geometric nonlinear formulation is almost the same as that by using the geometric linear formulation. These two solutions may deviate when the internal pressure of the containment p is greater than 1400 kPa. However, that is far beyond the internal pressure of interest $p =$ 886 kPa. Therefore, it can be concluded that when the containment fails, the deformation of the containment is still in a 'small' stage and the geometric nonlinear effect is negligible.

4.3. Influence of tension stiffening on the ultimate pressure capacity of containment

Fig. 10 shows the load-displacement curves of node 1 obtained by using different tension stiffening parameter ε^* (Fig. 6). When ε^* is set to a very small value close to the crack strain $\varepsilon_{cr} = f_t'/E_c$ of concrete, i.e. no tension stiffening, the ultimate pressure capacity of containment is 848 kPa, which should be the lower bound of the ultimate pressure. When the tension stiffening phenomenon is considered, the resulting ultimate pressure 886 kPa of the containment for $\varepsilon^* = 0.001$ is the same as that for $\varepsilon^* = 0.002$. Hence, as long as tension stiffening is properly taken into consideration, the influence of tension stiffening parameter on the ultimate pressure capacity of containment may not be significant.

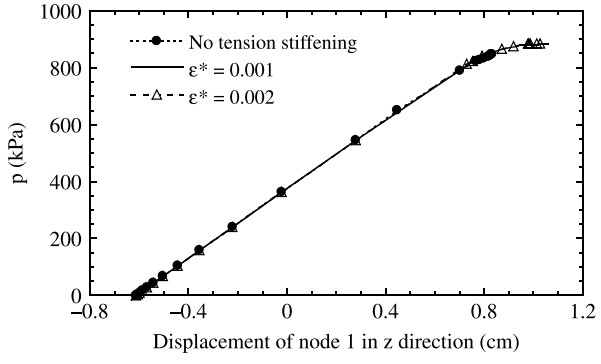

Fig. 10. Influence of tension stiffening on the ultimate pressure capacity of containment.

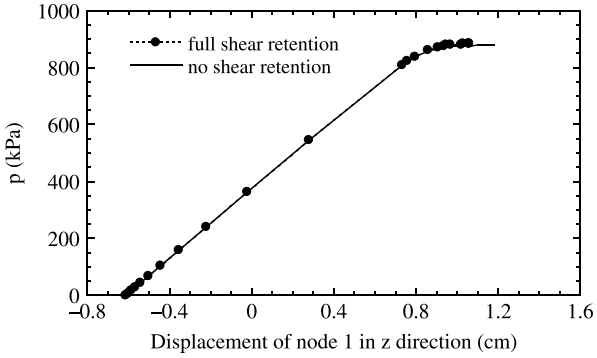

Fig. 11. Influence of shear retention on the ultimate pressure capacity of containment.

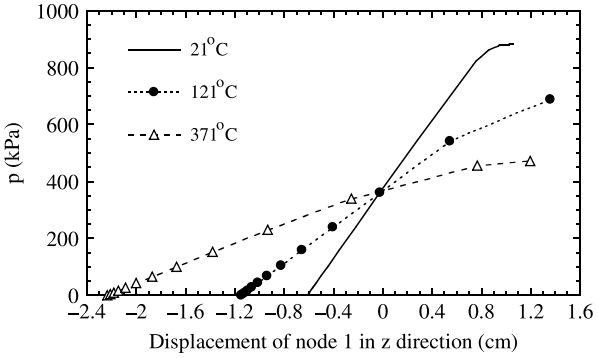

Fig. 13. Influence of temperature on the ultimate pressure capacity of containment.

4.4. Influence of shear retention on the ultimate pressure capacity of containment

Fig. 11 shows the load-displacement curves of node 1 obtained by using full shear retention and no shear retention. For full shear retention, the parameter μ is selected to be 1 (Fig. 7), and the shear modulus of cracked concrete is assumed to be the same as that of intact concrete. For no shear retention, the parameter μ is selected to be 0, and the shear modulus of cracked concrete is assumed to be zero. From the figure we can see that the load–displacement curves of these two extreme conditions are very close and similar. In addition, the difference of the ultimate pressure capacity for these two cases is small and within 0.5%. Hence, it can be concluded that shear retention has very little influence on the ultimate pressure capacity of containment.

4.5. Influence of base slab on the ultimate pressure capacity of containment

In previous sections, the containment in numerical analysis includes dome, cylinder and base slab. From Fig. 9 we can observe that under the ultimate internal pressure condition, the base slab has small deformation and major cracks occur at the dome and the bottom of cylinder. Hence, for the sake of saving computer time, it may be interesting to perform the finite element analysis again without the base slab and assume the cylinder to be clamped to the ground directly. Fig. 12 shows the load–displacement curves of the containment with and without base slab. It can be observed that the curve without base slab is stiffer than that with base slab. However, the ultimate pressure capacities for these two analyses are almost the same (0.5% difference). Under the ultimate pressure condition, the crack patterns for these two analyses are very similar except that the analysis without base slab has more cracks at the bottom of the cylinder [23]. Hence, for a rough and quick estimation of the ultimate load and the crack pattern, the base slab may be neglected.

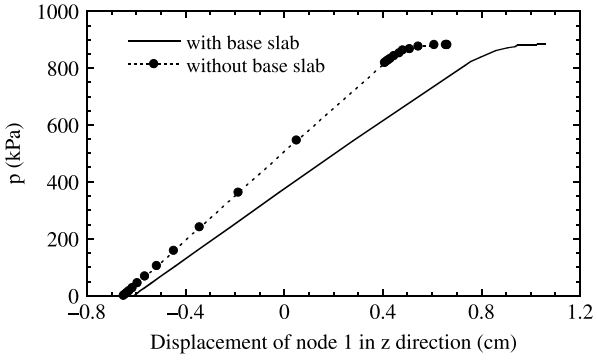

Fig. 12. Influence of base slab on the ultimate pressure capacity of containment.

4.6. Influence of temperature on the ultimate pressure capacity of containment

In this section, numerical analyses are carried out at the elevated temperature conditions (121 and 371 °C). For the sake of simplicity, heat transfer studies are not performed and the entire containment is assumed to be subjected to the same elevated temperature. Fig. 13 shows that the ultimate pressure capacity of the containment is 689 kPa under 121 °C temperature and is 472 kPa under 371 °C temperature. In addition, the stiffness of the containment is reduced with increasing temperature. From Tables 1 and 2, we can find that the degradations of the ultimate pressure capacity and the stiffness of the containment are primarily due to the weakening of concrete compressive strength f_c'. It should be noted that the ultimate pressure capacity of the containment under 371 °C temperature would be lower than the design load of 476 kPa.

5. Conclusions

From the nonlinear finite element analysis of the PWR prestressed concrete containment at Maanshan nuclear power plant, the following conclusions may be drawn:

(1) The ultimate pressure capacity of the containment is 886 kPa, which is about 86% higher than the design pressure of 476 kPa. Under the ultimate pressure condition, cracks are likely to occur near the apex of the dome, the junction of the dome and cylinder, and the bottom of the cylinder.
(2) When the containment fails, the deformation of the containment is still in a ‘small’ stage and the geometric nonlinear effect can be negligible.

(3) As long as tension stiffening is properly taken into consideration, the influence of tension stiffening parameter on the ultimate pressure capacity of containment may not be significant.
(4) Shear retention has very little influence on the ultimate pressure capacity of containment.
(5) For a rough and quick estimation of the ultimate load and the crack pattern, the base slab may be excluded from the ultimate analysis of the containment and the cylinder can be assumed to be clamped to the ground directly.
(6) The ultimate pressure capacity and the stiffness of the containment are significantly influenced by elevated temperature.

Acknowledgements

This research work was financially supported by the Atomic Energy Council of the Republic of China under Grant 842001NRD016.

References

[1] US Nuclear Regulatory Commission, Office of nuclear reactor regulation. Standard review plan for the review of safety analysis reports for nuclear plants, section 3.8.1, NUREG-0800; 1987.
[2] Amin M, Eberhardt AC, Erler BA. Design considerations for concrete containments under severe accident loads. Nucl Eng Des 1993;145:331–8.
[3] Boeck BD. A review of containment accidents. Nucl Eng Des 1993;145: 279–88.
[4] Rashid YR. Ultimate strength analysis of prestressed concrete pressure vessels. Nucl Eng Des 1968;7:334–44.
[5] Argyris JH, Gaust G, Szimmat J, Warnke EP, Willam KJ. Recent developments in the finite element analysis of prestressed concrete reactor vessels. Nucl Eng Des 1974;28:42–75.
[6] Connor JJ, Sarne Y. Nonlinear analysis of prestressed concrete reactor pressure vessels. Third international conference on structural mechanics in reactor technology, London, UK, vol. 3, H2/2; 1975.
[7] Goodpasture DW, Burdette EG, Callahan JP. Design and analysis of multicavity prestressed concrete reactor vessels. Nucl Eng Des 1978;46: 81–100.
[8] ASCE task committee on concrete and masonry structure. State of the art report on finite element analysis of reinforced concrete, ASCE; 1982.
[9] Chen WF. Plasticity in reinforced concrete. New York: McGraw-Hill; 1982.
[10] Meyer C, Okamura H. Finite element analysis of reinforced concrete structures. New York: ASCE; 1985.
[11] Hu H-T, Schnobrich WC. Nonlinear finite element analysis of reinforced concrete plates and shells under monotonic loading. Comput Struct 1991; 38:637–51.
[12] Borri A, Sorace S. FE analysis strategies for structural materials with small tensile strength. J Pressure Vessel Technol 1993;115:156–63.
[13] Pfeiffer PA, Kennedy JM, Marchertas AH. Post-test analysis for the nonlinear response of an internally pressurized one sixth scale reinforced concrete containment model. Nucl Eng Des 1992;133:143–57.
[14] Saito H, Muramatsu Y, Furukawa H, Hasegawa T, Mutoh A. Post-test of a 1:10-scale top slab model of ABWR/RCCV subjected to internal pressure. Nucl Eng Des 1993;145:339–53.
[15] Hu H-T, Liang JI. Ultimate analysis of BWR Mark III reinforced concrete containment subjected to internal pressure. Nucl Eng Des 2000;195:1–11.
[16] Hibbitt, Karlsson & Sorensen, Inc. ABAQUS/Standard user's manuals, Version 6.3, Providence, Rhode Island; 2003.
[17] ACI Committee 318. Building code requirements for structural concrete (ACI 318M-02) and commentary (ACI 318RM-02). American Concrete Institute, Detroit, MI; 2002.
[18] Nilson AH, Winter G. Design of concrete structures. 11th ed. New York: McGraw-Hill; 1991.
[19] Kupfer H, Hilsdorf HK, Rusch H. Behavior of concrete under biaxial stresses. ACI J 1969;66:656–66.
[20] Saenz LP. Discussion of 'Equation for the stress–strain curve of concrete'. Desayi P, Krishnan S, editors. ACI J 1964;61:1229–35.
[21] Pfeiffer PA, Kennedy JM, Marchertas AH. Thermal effects in the overpressurization response of reinforced concrete containment. Nucl Eng Des 1990;120:25–34.
[22] Taiwan Power Company. Final safety analysis report. Maanshan nuclear power station units 1 and 2, vol. 5; 1981.
[23] Lin Y-H. Analysis of the ultimate pressure capacity for a PWR prestressed concrete containment. MS thesis, Department of Civil Engineering, National Cheng Kung University, Tainan, Taiwan, ROC; 1995.